Fourier-Transform-Limited Performance of a Lithographically Scribed Planar Holographic Bragg Reflector

C. Greiner, D. Iazikov, and T. W. Mossberg

***Abstract*—Planar holographic Bragg reflectors (HBRs) are computer-generated two-dimensional (2-D) slab-waveguide-based refractive-index gratings. HBRs provide the spectral filtering function of fiber Bragg gratings but—enabled by the 2-D slab waveguide geometry—add the capability to spatially route signals. Here, we report on a silica-on-silicon-based focusing HBR providing 17 GHz, essentially Fourier-transform-limited, spectral resolution. This result comprises the first time deep ultraviolet projection lithography is successfully applied to the fabrication of a 2-D Bragg reflector on the centimeter scale. The 2-D Bragg filter occupies a compact 0.3 cm^2 footprint and provides diffraction-limited spatial input–output beam mapping.**

***Index Terms*—Integrated optics, volume hologram mode-specific photonic bandgap, waveguide grating.**

RECENTLY, it has been proposed [1], [2] and demonstrated [3] that slab-waveguide-based planar holograms, denoted two-dimensional (2-D) holographic Bragg reflectors (HBRs), offer the same spectral and spatial processing capabilities as fully three-dimensional volume holograms while, on the other hand, offering breakthrough pathways to fabrication. The planar HBRs of present concern consist of complex computer-generated 2-D gratings that are photolithographically scribed on the core of a slab waveguide. In the slab waveguide, light can propagate without constraints in two dimensions—a geometry that allows the 2-D Bragg structures to provide powerful planar holographic functions. A single HBR can simultaneously spatially map (image) an input beam onto an output port (or between active elements within an integrated photonic circuit) and provide spectral filtering. Stacking, interleaving, or overlaying of multiple HBRs [1], enabled by partial writing of diffractive contours, allows one to design multiport spectral processing devices, important, e.g., for spectral multiplexing, spectral signature recognition, and optical pulse shaping.

The holographic imaging function provided by HBRs enables free-space-like on-chip signal transport in which optical signals are allowed to freely overlap. This approach eliminates the need for constraining electronics-style channel waveguides and associated space requirements. Principally, holographic routing encompasses the capability of 90° signal routing, both in and (via higher order planar gratings) out of the waveguide plane. Out-of-plane coupling is important in laser feedback and outcoupling [4]–[6] or free-space to slab-waveguide beam coupling [7], [8]. Holographic imaging, furthermore, allows one to efficiently connect spatially extended input and output ports and is, thus, more powerful than confocal elliptical distributed Bragg reflectors [9] whose focusing power degrades when input and output optics deviate from the point source limit.

HBRs share similar physics with photonic crystals [10] and may indeed be viewed as a mode-specific type of photonic crystal [11]. Like photonic crystals, HBRs utilize refractive index variation to engineer optical field properties. Unlike photonic crystals, HBRs selectively engineer only those field modes specifically utilized in a photonic circuit function. The benefit accrued with selective mode control is compatibility with fabrication-friendly low index-contrast materials and structures. Being optical mode specific, HBR structures can be made physically large or small to accommodate required spectral resolution and available reflective scattering strengths. Ordinary photonic crystals, interacting with broad ranges of field modes [12]–[15], must utilize highly reflective (typically lossy and polarization sensitive) interfaces.

Owing to their planar, typically surface relief, structure, HBRs may be fabricated by deep ultraviolet (DUV) projection photolithography. In contrast to interference-based grating writing methods, e.g., using phase masks, holographic exposure or spatial frequency doubling lithography [9], [16] direct projection photolithography allows gratings to be written with complete amplitude and phase control over individual diffractive elements, a feature critical to flexible device apodization.

In this letter, we report on a HBR, fabricated by direct DUV projection lithography that provides 17-GHz, essentially Fourier-transform-limited, spectral resolution, which is substantially higher than previously reported [9]. The present device occupies a footprint of only 0.3 cm^2 and focuses the resonant input beam to a spatially distinct output with diffraction-limited performance.

Fig. 1(a) is a schematic top view of the HBR. The device was fabricated from a laser-written reticle employing a DUV optical stepper and standard etching, deposition, and annealing processes. An input beam is coupled into the device via an input channel waveguide, expands in the slab region, and interacts with the HBR. Wavelengths resonant with the HBR are spatially imaged to an output waveguide. The 2-D grating is 7 mm long and contains 13 305 lines. The overall device is 9 mm long (including the initial slab region) and 3 mm wide, resulting in a footprint of only about 0.3 cm^2. The access channel waveguides, spaced by $\Delta L = 400\,\mu$m, are located symmetrically about point C, and are angled (at their end points) by 2.275° with respect to the device optic axis (segment CD). The access channels are 6

Manuscript received July 18, 2003; revised November 19, 2003.

The authors are with the LightSmyth Technologies, Inc., Eugene, OR 97041 USA (e-mail: cgreiner@lightsmyth.com).

Digital Object Identifier 10.1109/LPT.2004.823700

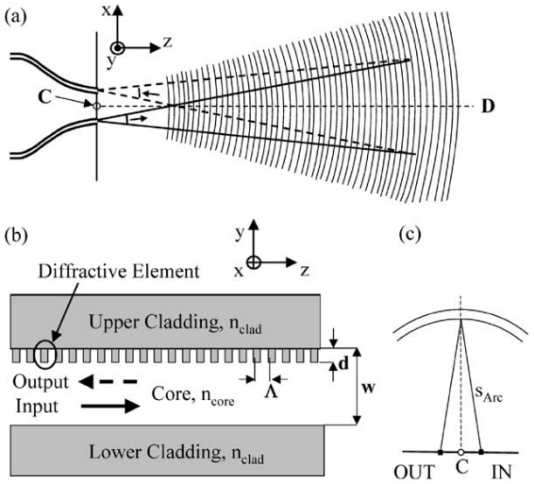

Fig. 1. Planar HBR schematics. (a) Top view. C: center of curvature of diffractive contours. The channel waveguides and the slab area to the right of the vertical line are regions with a high index core. (b) Cross-sectional view. W: waveguide width. D: grating depth. Λ: grating period. $n_{\rm core}$ $(n_{\rm clad})$: core (cladding) refractive index. (c) Schematic illustrating relation between device optic axis and optical path $s_{\rm Arc}$ to a given diffractive arc.

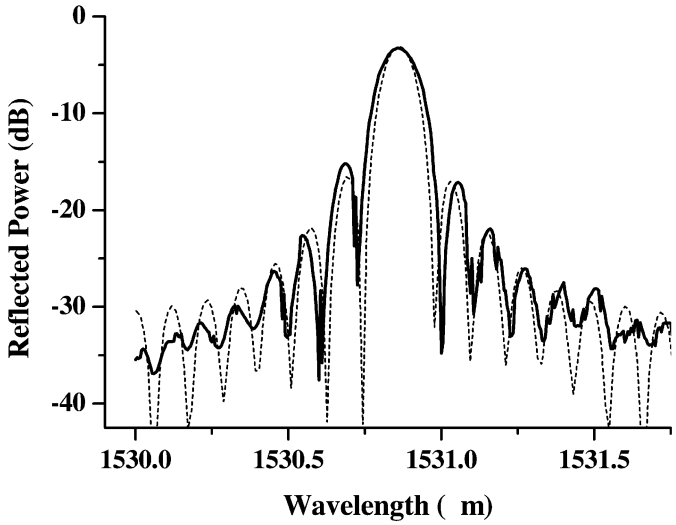

Fig. 2. Solid line: measured insertion loss versus wavelength for a 7-mm-long planar HBR (TE polarization). Dashed line: spectral transfer function calculated by Huygens–Fresnel diffraction theory.

μm at the die edge and taper over 1 mm to a 12.7-output width. The HBR intercepts 99.8% of the input beam's total power. Nonresonant light leaves the HBR region without being spatially redirected. Collection of this express signal are discussed elsewhere [17].

The HBR diffractive contours, represented in Fig. 1(a) by thin solid lines, can be designed individually to optimally match the back-diffracted input field to the output port. In the tested device, the contours are circular arcs which are concentric about point C, the center of curvature. Computer-generated holographic contours will improve input–output coupling through optimization of spatial wavefront transformation and are equally enabled by the currently demonstrated spatial coherence.

Adjacent diffractive arcs are spaced such that the optical path length $s_{\rm Arc}$, as shown in Fig. 1(c), is incremented by a constant amount $\Lambda = \lambda_0/2n_{\rm eff}$ from one arc to the next. Here, λ_0 is the designed resonance wavelength and $n_{\rm eff}$ is the effective waveguide refractive index. Since $s_{\rm Arc}$ and the device optic axis (segment CD) are not quite parallel, the spacing between adjacent arcs, as measured along the optic axis, is weakly chirped. The radius of the first diffractive arc is 2 mm.

Fig. 1(b) shows a schematic partial cross section of the device. It consists of a silica slab waveguide fabricated by depositing a 6-μm–thick central core of $+0.8\%$ index contrast on a 15-μm-thick undercladding and covering it, through deposition, with an equally thick upper cladding. Fig. 1(b) also depicts cross sections of representative lithographically scribed diffractive contours located at the upper core–cladding interface. The diffractive contours, with depth $d \approx 450$ nm, consist of trenches filled with cladding material. The device operates in first order with a contour spacing Λ of about 500 nm, i.e., one half of the in-medium wavelength of resonant light. In the schematic cross section of Fig. 1(b), light enters the device from the left side and is backscattered by the diffractive elements.

In Fig. 2, we present (solid line) the HBR spectral transfer function for transverse-electric (TE) input polarization, measured by use of a tunable laser. The resonant insertion loss of the device was measured to be $+3.1$ dB. A fiber-to-slab-waveguide coupling loss of $+1.4$ dB is subtracted from the results shown in Fig. 2. As seen in Fig. 2, the 7-mm-long HBR has a spectral full-width at half-maximum of $\sim$0.13 nm, corresponding to a fractional spectral resolution $\Delta\lambda/\lambda$, better than 10^{-4}, close to the Fourier-transform-limited fractional bandpass of 7.5×10^{-5}, calculated for a one-dimensional (1-D) grating with 13 305 grating lines. The result of Fig. 2 indicates that the lithographic fabrication process provides control at the same level of precision over reduction ratio, feature placement, and index homogeneity over the device length. The accuracy of the measured center wavelength of $\sim$1.5308 μm as compared to the design value of 1.530 37 μm is better than 3×10^{-4} and can be improved using the present results as calibration.

We have applied 2-D Huygens–Fresnel diffraction theory to the full HBR structure to calculate its expected reflection spectrum in the weak reflection limit. The result is shown in Fig. 2 as the dashed line. An input field with Gaussian transverse distribution (1/e-diameter 12 μm), approximating the modal field of the experiment, was assumed. Interestingly, a 1-D coupled-mode analysis yields an essentially identical low reflectivity result. While our Huygens–Fresnel 2-D model is not easily extendable to the finite reflectivity limit, the 1-D coupled-mode calculation is. When used to simulate the reflection spectrum of a 1-D grating of having our measured reflectivity, the width of the reflection spectrum is found to match the experimentally measured width. The result of Fig. 2 conclusively demonstrates that the silica-on-silicon format and submicron lithographic fabrication can provide fully coherent planar holographic structures of centimeter scale.

In Fig. 3(a), we explore the focusing properties of the fabricated HBR. For these measurements, the device die are cut (30 μm) along the vertical line shown in Fig. 1(a) so that the die edge contains point C and lies normal to the optic axis. No channel waveguides are present. One butt-coupled SMF-28 fiber (manufacturer specified core and mode field diameters of 8.2 and 10.4 μm, respectively) is positioned approximately

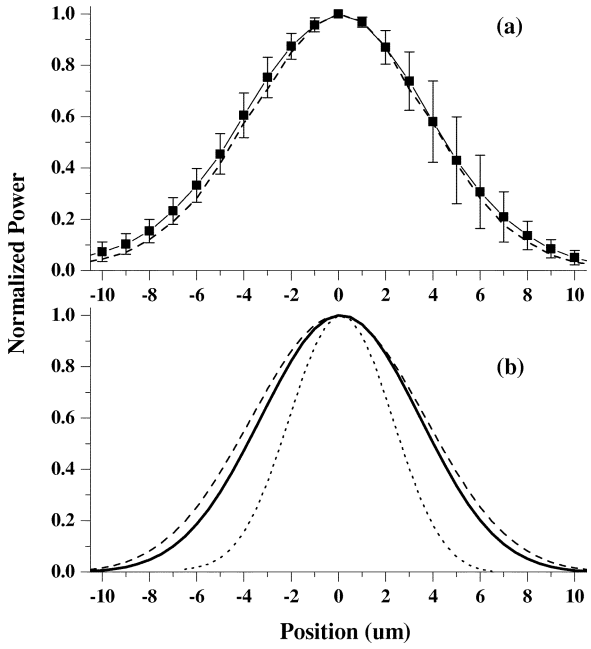

Fig. 3. Measured and calculated HBR output spatial profiles. (a) Squares: HBR data. Dashed line: measured input fiber spatial power profile. (b) Solid line: calculated HBR spatial output profile. Dashed line: calculated input spatial power profile. Dotted line: calculated unconvolved HBR output profile.

200 μm to one side of point C and is used to inject signal. A second butt-coupled SMF-28 fiber is scanned parallel to the die edge about 200 μm to the opposite side of point C (position 0). Squares and error bars on the solid line in Fig. 3 represent mean power and standard deviation of five HBR measurements. Also shown, as a dashed line, is the output power profile of the SMF-28 input fiber measured by scanning a second fiber directly across its face. With perfect HBR imaging of input to output, the solid and dashed lines should agree as they do.

We employed 2-D Huygens–Fresnel diffraction theory to simulate the HBR spatial output profile. The input and measurement fiber modes were modeled by a Gaussian function of 1/e-field diameter 10.4 μm. The dotted line in Fig. 3(b) represents the calculated spatial HBR output power profile. The solid line shows the model HBR output power profile as expected after convolution with the response of the measurement fiber. The dashed line represents the input fiber power profile as it would be measured after convolution with a measurement fiber. As can be seen, the convolved power profiles of the modeled HBR output and input fiber are very similar in shape and width, which is consistent with diffraction-limited, unity conjugate ratio, imaging data.

For the present device, insertion loss is limited by the coupling strength of its diffractive elements. Detailed calculations [18] indicate that achievable alterations in diffractive structure geometry and refractive-index contrast will lead to HBRs of centimeter-scale having strong reflectivity and, thus, low insertion loss over an aggregate bandwidth as large as several hundred nanometers. In the high reflectivity limit, the extensive set of design tools developed in the context of apodized fiber Bragg gratings [19], [20] can be readily implemented.

In conclusion, we have demonstrated lithographically fabricated silica-on-silicon-based HBRs that provide spectral filtering performance and spatial beam mapping constrained only by the fundamental limits of Fourier transform and diffraction theory. We envision HBRs as a "photonic fabric" that not only provides optics-on-a-chip functions such as multiplexer–demultiplexer, spectral LED slicing, laser wavelength locking, and cross-correlation-based header recognition but also provides for the integration of these functions into a single compact photonic circuit format, especially when implemented in active materials.

REFERENCES

[1] T. W. Mossberg, "Planar holographic optical processing devices," *Opt. Lett.*, vol. 26, pp. 414–416, 2001.
[2] ——, "Lithographic holography in planar waveguides," *SPIE Holography Newsletter*, vol. 12, pp. 1 –8, 2001.
[3] C. Greiner, D. Iazikov, and T. W. Mossberg, "Lithographically scribed, focusing, planar holographic Bragg reflector with 17-GHz passband and 0.3 cm^2 footprint," in *Optical Fiber Communication Conf.*, Atlanta, GA, Mar. 23–28, 2003, Postdeadline Paper PD31.
[4] T. Erdogan and D. G. Hall, "Circularly symmetric distributed feedback laser: Coupled mode treatment of TE vector fields," *IEEE J. Quantum Electron.*, vol. 28, pp. 612–623, Mar. 1992.
[5] R. H. Jordan, D. G. Hall, O. King, G. Wicks, and S. Rishton, "Lasing behavior of circular grating surface emitting semiconductor lasers," *J. Opt. Soc. Amer. B*, vol. 14, pp. 449–453, 1997.
[6] S. Kristjansson, N. Eriksson, A. Larsson, R. S. Penner, and M. Fallahi, "Observation of stable cylindrical modes in electrically pumped circular grating-coupled surface-emitting lasers," *Appl. Opt.*, vol. 39, pp. 1946–1953, 2000.
[7] M. Li, B. S. Luo, C. P. Grover, Y. Feng, and H. C. Liu, "Waveguide grating coupler with a tailored spectral response based on a computer-generated waveguide hologram," *Opt. Lett.*, vol. 24, pp. 655–657, 1999.
[8] J. Backlund, J. Bengtsson, C. Carlstrom, and A. Larsson, "Input waveguide grating couplers designed for a desired wavelength and polarization response," *Appl. Opt.*, vol. 41, pp. 2818–2825, 2002.
[9] C. H. Henry, R. F. Kazarinov, Y. Shani, R. C. Kistler, V. Pol, and K. J. Orlowsky, "Four-channel wavelength division multiplexers and bandpass filters based on elliptical Bragg reflectors," *J. Lightwave Technol.*, vol. 8, pp. 748–755, May 1990.
[10] J. D. Joannopoulos, R. D. Meade, and J. N. Winn, *Photonic Crystals. Molding the Flow of Light*. Princeton, NJ: Princeton Univ. Press, 1995.
[11] A. Yariv and P. Yeh, *Optical Waves in Crystals*. New York : Wiley, 1984.
[12] D. Labilloy, H. Benisty, C. Weisbuch, T. F. Krauss, D. Cassagne, C. Jouanin, R. Houdre, U. Oesterle, and V. Bardinal, "Diffraction efficiency and guided light control by two-dimensional photonic-bandgap lattices," *IEEE J. Quantum Electron.*, vol. 35, pp. 1045–1052, July 1999.
[13] A. Giorgio, A. G. Perri, and M. N. Armenise, "Modeling of fully etched waveguiding photonic bandgap structures," *IEEE J. Quantum. Electron.*, vol. 38, pp. 630–639 , June 2002.
[14] D. M. Pustai, A. Sharkawy, S. Shi, G. Jin, J. Murakowski, and D. W. Prather, "Characterization and analysis of photonic crystal coupled waveguides," *J. Microlith. Microfab. Microsyst.*, vol. 2, pp. 293–298, 2003.
[15] S. Rowson, A. Chelnokov, and J. M. Lourtioz, "Two-dimensional photonic crystals in macroporous silicon: From mid-infrared (10 μm) to telecommunication wavelengths (1.3–1.5 μm)," *J. Lightwave Technol.*, vol. 17, pp. 1989–1995, Nov. 1999.
[16] T. E. Jewell and D. L. White, "Spatial frequency doubling lithography (SFDL) of periodic structures for integrated optical circuit technology," *J. Lightwave Technol.*, vol. 7, pp. 1386–1393 , Sept. 1989.
[17] C. Greiner, D. Iazikov, and T. W. Mossberg, "Lithgraphically fabricated planar holographic Bragg reflectors," *J. Lightwave Technol.*, to be published.
[18] ——, "Apodizable integrated filters for coarse WDM and FTTH-type applications ," *J. Lightwave Technol.*, to be published.
[19] R. Feced, M. N. Zervas, and M. A. Muriel, "An efficient inverse scattering algorithm for the design of nonuniform fiber Bragg gratings," *IEEE J. Quantum Electron.*, vol. 35, pp. 1105–1115, Aug. 1999.
[20] J. Skaar, L. Wang, and T. Erdogan, "On the synthesis of fiber Bragg gratings by layer peeling," *IEEE J. Quantum Electron.*, vol. 37, pp. 165–173, Feb. 2001.